JTTEE5 5:175-184


# Numerical Analysis of a High-Velocity Oxygen-Fuel Thermal Spray System

*X. Yang and S. Eidelman*

**The fluid and particle flow field characteristics of a high-velocity oxygen-fuel (HVOF) thermal spray (TS) system are analyzed using a two-phase flow model and simulated using computational fluid dynamics (CFD) techniques. The model consists of a conservation equation and constitutive relations for both gas and particle phases. Compressible, turbulent flow is modeled by a $k$-$\varepsilon$ turbulent model. A Lagrangian formulation is used to model particle trajectory, and heat and momentum transfer. The fluid velocity fluctuations resulting from gas turbulence are simulated by a stochastic model and the particle motion in the turbulent flow is calculated in a Lagrangian Stochastic-Deterministic (LSD) method. Details of gas flow field, particle temperature and particle velocity histories, and particle temperature and velocity profiles in the system are presented. For the validation of the numerical analysis, the computed results are compared with available experimental measurement. Excellent agreement between simulations and measurements is obtained for both gas and particle flow fields. A parametric study is also conducted for different particle sizes and different nozzle barrel lengths. The flow phenomena for different flow parameters are analyzed and explained as the result of gas dynamics and heat and momentum transfer between the two phases. The developed methodology provides a means to analyze, design, and optimize the TS process. The numerical analysis presents a first comprehensive, fundamental quantitative analysis for the HVOF TS system.**

## 1. Introduction

THE HIGH-VELOCITY oxygen-fuel (HVOF) thermal spray (TS) system has been used in the aerospace industry for a variety of surface coating applications for many years. Aerospace engineers use TS coatings to insulate parts from heat, reduce turbine blade wear, and protect against oxidation and corrosion (Ref 1). Although the process is widely used, TS system design has been primarily empirical and the understanding of the system mechanism is based on engineering intuition and analysis of operational data. The schematic diagram of the system, including combustion chamber, nozzle, barrel, particle injection, gas and particle flow field, is shown in Fig. 1. High-pressure and high-temperature combustion gases resulting from the combustion of oxygen and fuel expand through the converging and diverging de Laval nozzle and the barrel to supersonic speed (local Mach number $M \approx 2$). Particles are then injected into the barrel at the exit of the nozzle. Particles are turbulently mixed, heated, and accelerated in the barrel and jet at high speed and temperature to the substrate to be coated. From the fluid dynamics point of view, the system is very complex and involves two-phase (gas-particle) flow with turbulence, heat transfer, chemical reactions, and supersonic/subsonic flow transitions. In an engineering application, the microstructure and physical properties of the plated surface are determined by the physical and chemical conditions of the particles that impinge on the surface. The physical and chemical condition of the particle impinging on the substrate in turn is dependent on a large number of parameters such as gun design (length of barrel in particular), the gas jet formation, the position of the particle relative to the substrate, the particle size, shape, material, injection method, and so forth. In recent years, some publications have been dedicated to analyzing the TS process (Ref 2-4). However, these studies are either based on some highly simplified model or address only the gas and particle flow in the jet, without considering the key processes of particle injection and gas/particle flow inside barrel.

**Keywords** high-velocity oxygen-fuel, Lagrangian formulation, particle trajectory, particle temperature, supersonic, thermal spray, two-phase flow, turbulent flow

**X. Yang** and **S. Eidelman,** Science Applications International Corporation, McLean, VA, USA.

To advance the technology of the TS system and improve the quality and efficiency of the TS coating, we believe that a detailed understanding of the complete system is needed. The understanding will include gas dynamics, particle injection, the interaction between the injected particle and gas flow, particle conditions before they impinge on the substrate, and the relation of the particle condition to the final coating quality. In this paper, we present a study of the HVOF thermal spray system using computational fluid dynamics. We first formulate the compressible two-phase flow using a Eulerian (for gas) and Lagrangian (for particle) formulation. The dynamics of the flow are governed by conservation equations of each phase, and the particle phase is coupled with gas phase by momentum and heat transfer. We solve the system of equations numerically for the gas and particle flow field. The objectives of the study are (1) to formulate and solve the HVOF TS flow field and compare the simulation with existing experimental results and (2) to conduct a parametric study using a validated model to explore the characteristics of the two-phase flow for TS engineering applications.

## 2. Mathematical Model and Numerical Solution

The mathematical model for the two-phase flow consists of a conservation-governing equation and constitutive relations that provide closure models. The basic formulation adopted here follows the gas and low-loading particle flow dynamics model presented by Crowe et al. (Ref 5) and Chen and Crowe (Ref 6). For

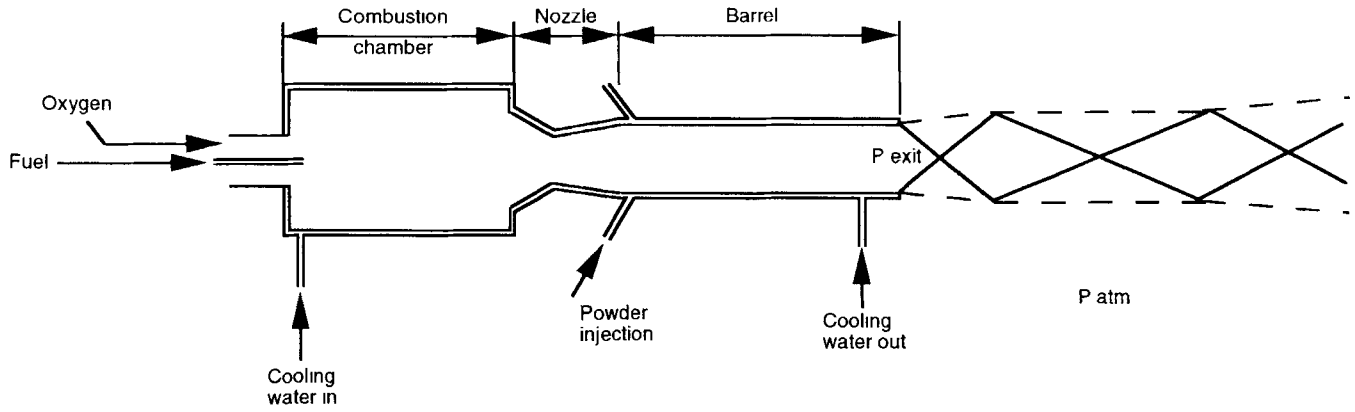


**Fig. 1** Schematic of the high-pressure HVOF gun and flow field

the gas flow, it is natural to use the Eulerian approach for analyzing the continuum. A direct numerical simulation of the two-phase turbulent flow system requires solving the instantaneous compressible Navier-Stokes equation for the gas flow followed by simulating the motion of a large number of particles in the resolved instantaneous gas field. This method needs large capacity and very fast computers. It is not practical at the present time for engineering applications. At present, it is more appropriate to apply an averaged Navier-Stokes equation with turbulence models. In this study, the gas model is the compressible Navier-Stokes equation in Favre mass-averaged variables for the conservation of mass, momentum, and energy. To model flow turbulence, the Reynolds stress tensor is closed using a $k$-$\varepsilon$ turbulence model (Ref 7). Here, $k$ is turbulent kinetic energy and $\varepsilon$ is the rate of dissipation of kinetic energy. A recently developed (Ref 8) three-dimensional, multiblock, upwind, fully implicit, finite volume code was modified to solve the governing equations. The code incorporates the high-order, upwind, flux-difference splitting process of Roe (Ref 9) with a monotonic upstream-centered scheme for conservation laws (MUSCL) integration scheme to obtain good shock-capturing, high-accuracy solutions in general coordinates for the three-dimensional geometry computational domain. For a three-dimensional flow, seven variable-governing equations are discretized and integrated in time to provide a steady-state solution. To deal with the well-known stiffness of the equations, an implicit time integration is used. The details of the code and numerical solution techniques can be found in Ref 7.

To describe particle motion, we use the Lagrangian formulation. The Lagrangian formulation allows a description of the particle/wall interactions that are very difficult to analyze numerically using a Eulerian approach. In addition, the Lagrangian formulation is also logical for the low-volume, collisionless particle flow that is typical of TS systems. To simplify the analysis, the following assumptions are made:

- The particles do not undergo a phase change.
- The particles are solid spheres and have a constant material density.
- The volume occupied by the particles is negligible.
- The interaction between particles can be ignored.
- The only force acting on a particle is drag force, and the only heat transfer between the two phases is convection.
- The weight of the solid particles and their buoyancy force are negligible compared to the drag force.
- The particles have a constant specific heat and are assumed to have a uniform temperature distribution inside each particle.

Furthermore, because the loading of the particle defined as total mass flow rate/total gas mass flow rate is very low (<4%), one can assume that the presence of particles will have a minimal effect on gas velocity and temperature field. This means that the momentum and heat exchanges from particle to gas are too small to change gas velocity and temperature distribution. As a result of the assumptions presented above, the two-phase problem can then be decoupled: The gas flow field can be simulated first, followed by the particle flow analysis.

The simulation of the particle flow field consists of calculating particle trajectories and temperature histories in the gun barrel and in the jet, after particles are injected into the gun barrel from the particle injection port. The interaction between particle and wall is also included in the simulation.

Particle motion in gas turbulent flow is predicted by means of the Lagrangian stochastic model (LSD) (Ref 10, 11). There are two elements in the LSD model: the description of the turbulent field and integration of the particle motion equations.

The numerical solution of gas fluid equations provides the fields of mean velocity components as well as turbulent kinetic energy $k$ and dissipation rate of turbulent kinetic energy, $\varepsilon$. From $k$ and $\varepsilon$, the scales in time and space of large turbulence eddies can be evaluated. The fluid instantaneous velocity is obtained by adding the fluctuating velocity resulting from large turbulent eddy to the mean velocity. The root mean fluctuating velocity can be calculated from turbulent kinetic energy $k$, which is defined as $\vec{V'}\vec{V'}/2$, where $\vec{V'}$ is fluctuating velocity defined as $\vec{V'} = (u'\vec{i} + v'\vec{j} + w'\vec{k})$. If the turbulent field is assumed to be isotropic and to possess a Gaussian distribution of fluctuating velocity, then the turbulent kinetic energy $k$ is equal to $\frac{1}{2}(u'^2 + v'^2 + w'^2) = \frac{3}{2}u'^2$. The standard deviation of the fluctuating velocity distribution is $\sigma' = (3k/2)^{1/2}$.

Using this standard deviation and the assumption of a Gaussian and isotropic distribution of fluctuating velocities, we can

calculate turbulent velocity fluctuation. The instantaneous total fluid velocity is then:

$$\vec{V}_g = \vec{U}_g + \vec{V}' \quad \text{(Eq 1)}$$

where $\vec{U}_g$ is the mean flow velocity.

The equation of motion for a particle in the gas flow (Ref 5) is

$$m_p \frac{d\vec{V}_p}{dt} = C_D \rho_g \left(\vec{V}_g - \vec{V}_p\right) \left| \vec{V}_g - \vec{V}_p \right| \frac{A_p}{2} + \vec{F} \quad \text{(Eq 2)}$$

where $\rho_g$ is gas intensity, $m_p$ is particle mass, $\vec{V}_p$ and $\vec{V}_g$ are particle and gas velocity vectors, respectively. $A_p$ is the particle area. The term $\vec{F}$ denotes external force like gravity or centrifugal or Coriolis force in a cylindrical coordinate system. Other forces such as added mass effect and Basset history force are not presently considered because they are of the order of the gas/particle density ratio, which for most applications of interest is of the order of $10^{-3}$ (Ref 12, 13).

The drag coefficient, $C_D$, which appears in Eq 2, depends on a few parameters, for example, the Reynolds number, the Mach number, the surface roughness of the particle, the flow stream turbulence level, the rotation of the particle, and so forth. However, it depends primarily on the Reynolds number. For the present solution, the simple form proposed in Ref 14 is adopted:

$$C_D = \left(\frac{24}{Re_p}\right)\left(1 + 1.015\, Re_p^{0.687}\right) Re_p < 1000$$

$$C_D = 0.44 \quad Rep > 1000 \quad \text{(Eq 3)}$$

Here the particle Reynolds number is defined by

$$Re_p = \rho_g \frac{\left(\left| \vec{V}_g - \vec{V}_p \right|\right)}{\mu_g} d_p \quad \text{(Eq 4)}$$

where $U_g$ is gas viscosity.

Integrating Eq 1, assuming the gas velocity is constant over the time of integration and defining $f = C_d\, Re/24$, yields

$$\vec{V}_p = \vec{V}_g - \left(\vec{V}_g - \vec{V}_p^o\right) \exp\left(\frac{-\Delta t}{\tau}\right) \quad \text{(Eq 5)}$$

where $\vec{V}_p^o$ is the initial particle velocity, $\Delta t$ is the time interval, and $\tau$ is

$$\tau = \frac{\rho_s d_p^2}{18 \mu_g f} \quad \text{(Eq 6)}$$

where $\rho_s$ is particle material density.

After calculating the particle velocity, the particle position at time $\Delta t$ is determined as:

$$\vec{X} = \vec{X}_o + \left(\vec{V}_p + \vec{V}_p^o\right) \frac{\Delta t}{2} \quad \text{(Eq 7)}$$

The model assumes that the particle interacts with a sequence of turbulent eddies of given size and lifetime. After the particle traverses the eddy or the eddy dissipates, we assume that the particle enters a new eddy with a randomly sampled new fluctuation intensity and hence, a given size and dissipation time. As a result, the interaction time (the $\Delta t$ in Eq 5) is the minimum of turbulence dissipation time and the time required for the particle to traverse a given eddy.

The characteristic size of the randomly sampled turbulent flow field (eddy size) is proportional to turbulent length scale given by $l_e = ck^{3/2}/\varepsilon$. Here $\varepsilon$ is the energy dissipation rate that was calculated from the $k$-$\varepsilon$ model in gas turbulent flow calculation. $c$ is equal to 0.3 according to arguments in Ref 10. The eddy lifetime is estimated as $\Delta t_e = l_e/|\vec{V}'|$.

The requirement that the particle must remain within the eddy during the interaction time interval leads to the second part of the requirement that

$$\Delta t_r \le \frac{l_e}{\left|\vec{V}_g - \vec{V}_p\right|}$$

Therefore, the interaction time between particle and gas (the eddy) will be the minimum of $\Delta t_e$ and $\Delta t_r$; that is, $\Delta t = \text{Min}(\Delta t_e, \Delta t_r)$. After one interaction time, a new velocity fluctuation is randomly sampled and the process is repeated.

The governing equation to calculate particle temperatures is:

$$m_p C_p \frac{dT_p}{dt} = \dot{q} \quad \text{(Eq 8)}$$

where $C_p$ is the specific heat of the particle and $\dot{q}$ is the heat transfer rate to the particle. The rate of heat transfer excluding radiation heat transfer is defined as:

$$\dot{q} = Nu \pi k_g d_p \left(T_g - T_p\right) \quad \text{(Eq 9)}$$

where $k_g$ is the thermal conductivity of the gas and Nu is the Nusselt number and is a function of the Reynolds number and Prandtl number. The relation used here is:

$$Nu = 2 + 0.6 Re^{0.5} Pr^{0.33} \quad \text{(Eq 10)}$$

Integrating the particle heat transfer equation over a small time interval, $\Delta t$, and assuming a gas temperature constant over the integration time, $\Delta t$, the resulting particle temperature is

$$T_p = T_g - \left(T_g - T_p^o\right) \exp\left(-\frac{\Delta t}{\sigma}\right) \quad \text{(Eq 11)}$$

where $\sigma$ is defined as

$$\sigma = \frac{\rho_s d_p^2 C_p}{6 Nu \cdot k_g} \quad \text{(Eq 12)}$$

## 3. Results

### 3.1 *Gas Flow Simulations*

To validate the current two-phase flow model and numerical solution procedure, we selected the TAFA JP-5000 HVOF TS system (Ref 15) as the test case because extensive experimental data are available for this system. We first resolve the gas flow field in the barrel. The chemical state of the gas flow in the barrel

can be considered to be in equilibrium or frozen composition. Experimental measurements (Ref 16) indicate that the flow is closer to the frozen state than to equilibrium. This is because the gas residence time is shorter than the chemical reaction time. Thus, we assumed in our simulations that the gas has a frozen chemical composition for a given fuel/oxygen ratio. The state of gas in a frozen condition can be calculated using the NASA Gordon-McBride program (Ref 17). We simulated the JP-5000 gun flow for the conditions given in Ref 16, for which the experimental measurements were made. We considered the gas flow for the TAFA JP-5000 gun (Hobart Tafa Technologies Inc., Concord, NH) with a 200 mm (8 in.) barrel with the following conditions in the combustion chamber:

- Molar mass of combustion products: $M$ = 25.84 kg/kg mole
- Stagnation temperature: $T^o$ = 3100 K
- Chamber pressure: $p^o$ = 586.1 kPa
- Isentropic coefficient: $\alpha$ = 1.12

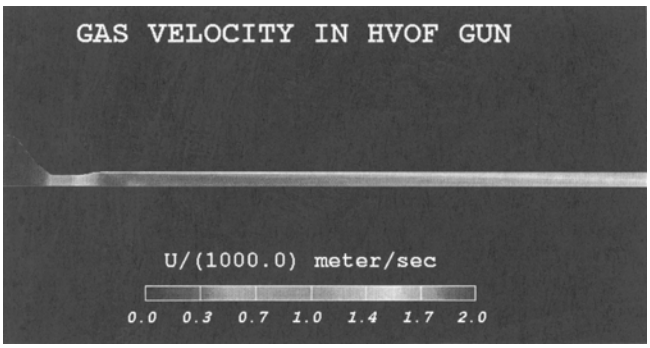


**Fig. 2** Velocity contours inside the nozzle and barrel of the gun

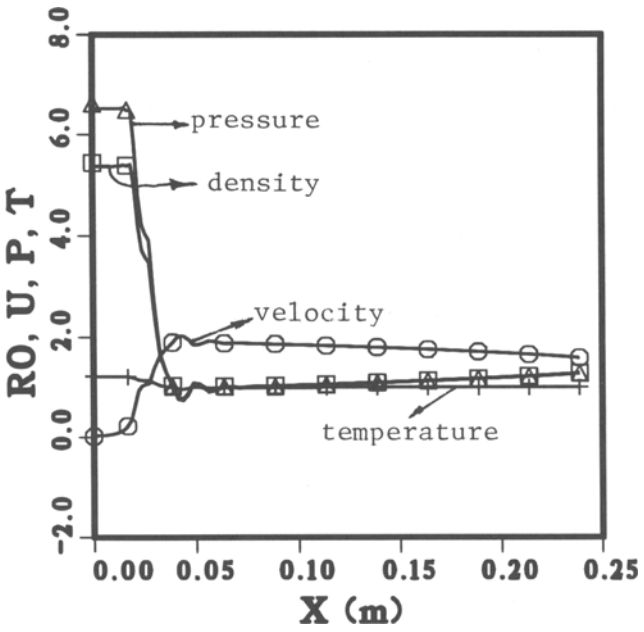


**Fig. 3** Properties along the nozzle and barrel centerline. Density (□, $\rho/\rho_{Ref}$, $\rho_{Ref}$ = 0.121 kg/m$^3$); velocity (○, $u/a_{Ref}$, $a_{Ref}$ = 966 m/s); pressure (Δ, $p/p_{Ref}$, $p_{Ref}$ = 101,325 Pa); temperature (+, $T/T_{Ref}$, $T_{Ref}$ = 2600 K)

Given these conditions and the gun/barrel geometry, we simulated the steady-state flow regime for the gun de Laval nozzle and barrel, using barrel lengths of 8 and 4 in. The results for the 8 in. length are shown as velocity contour plots in Fig. 2, which shows flow acceleration in the de Laval nozzle from very low subsonic speeds on the order of less than 1 m/s in the combustion chamber to high supersonic speeds on the order of 2000 m/s in the barrel. We also notice that a significant boundary layer develops in the barrel. This leads to a decay of flow velocity along the barrel because of partial constriction of the channel. The nondimensional pressure, temperature, and velocity distribution along the nozzle and barrel centerline is given in Fig. 3. Here the following trends can be noted:

- The pressure and density drop rapidly in the de Laval nozzle, reaching a minimum and then steadily increasing along the barrel length with the reduction of flow velocity.
- The velocity increases to 2000 m/s at the nozzle exit and then gradually decreases to 1700 m/s at the barrel exit as a result of the boundary layer growth.
- The temperature decreases from 3100 K in the chamber to about 2500 K at the barrel exit.

Figure 4 compares the simulation results in the form of velocity distribution at the barrel exit with the experimentally measured values given in Ref 16 and shows an excellent agreement between the computational and experimental results, indicating that our numerical methodology can accurately predict the flow regimes of the TS guns. The maximum deviation between numerical and experimental results shown in Fig. 4 is less than 10%. Figure 5 shows the comparison between computational prediction and experimental measurements of radial distribution of gas temperature at barrel exit. Again, good agreement between experimental and numerical results is observed.

The external flow field is calculated with the flow condition at the exit of the gun barrel as the input boundary condition for jet simulation in the ambient air. Because the pressure at the barrel exit is greater than the ambient pressure, the nozzle flow is categorized to be underexpanded. The flow expands supersonically into the ambient air. The density contour plot for the jet is shown in Fig. 6. The jet flow forms a supersonic core region, generates a so-called diamond shock pattern of expansion and compression waves, forms a free shear layer between jet and external air, and mixes and entrains the ambient air into the jet to slow down the jet from supersonic flow to subsonic flow. Figure 6 shows the jet cross-section growth as a result of mixing with the external air. Currently, the only quantitative experimental measurements of such jets are given in Ref 16, which presents measurements of velocity at the jet centerline. Figure 7 compares the velocity data obtained from our simulation with the experimental measurements given in Ref 16 for the same conditions. We can see from this comparison that experimental observations validate our simulations, and the deviation between the numerical and experimental data is less than 10%.

### 3.2 *Particle Flow Simulations*

As discussed in the last section, the loading (defined as particle mass flow rate/gas mass flow rate) is low (<4%). The pres-

ence of particle flow will not influence the gas flow field. After calculating the gas flow field, we integrate the equation of particle motion (Eq 2) and the equation of heat transfer (Eq 8) to obtain particle trajectories and temperature histories for different particle diameters and injection speeds. Inconel 718 particles are used in the study. The following particle flow parameters are selected for the test cases:

- Particle material density: $\rho_s = 9000$ kg/m$^3$
- Particle diameters: $D_p = 10\ \mu m, 20\ \mu m, 40\ \mu m, 60\ \mu m$
- Specific heat: $C_s = 462$ J/kg·K
- Injection angle: $\alpha = 12° \pm 5°$
- Injection speed: $u_j = 20$ m/s

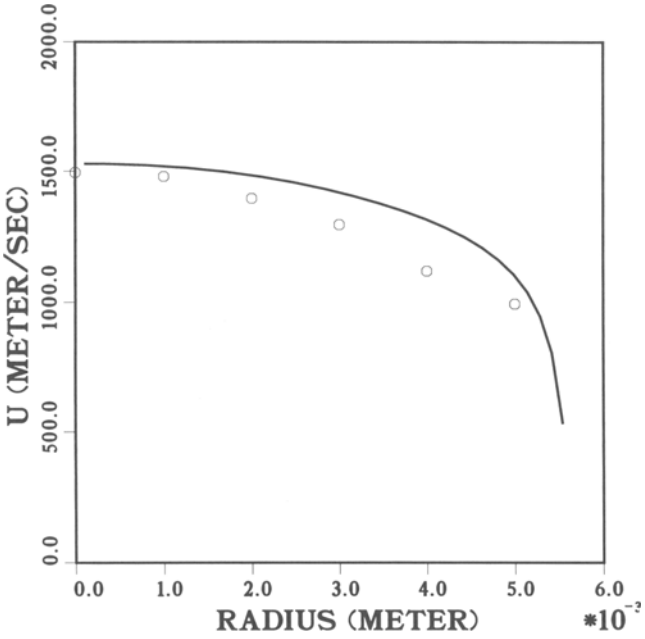


**Fig. 4** Comparison between computational prediction and experimental measurement of radial distribution of gas velocity (O, experiment, Ref 16; ——, calculation), at barrel exit

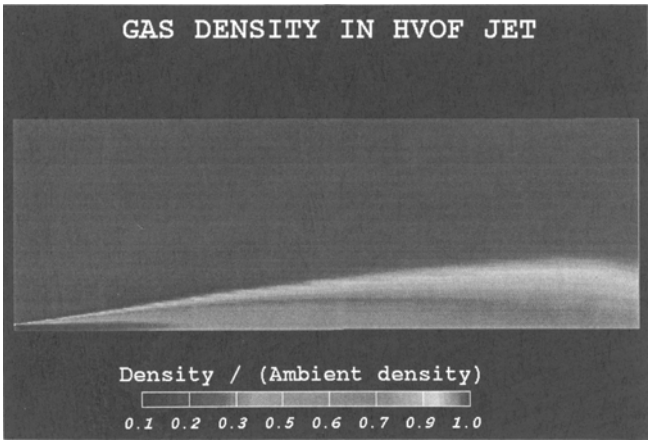


**Fig. 6** Density contours in the area of the barrel and the jet for the JP-5000 gun

A large number (>1000) of particle trajectories and temperature histories are traced through the flow field (from nozzle injection to plating distance) in order to obtain mean particle flow properties.

The first set of simulations was done for particles injected into the barrel at a speed of 20 m/s for an 8 in. barrel gun. Be-

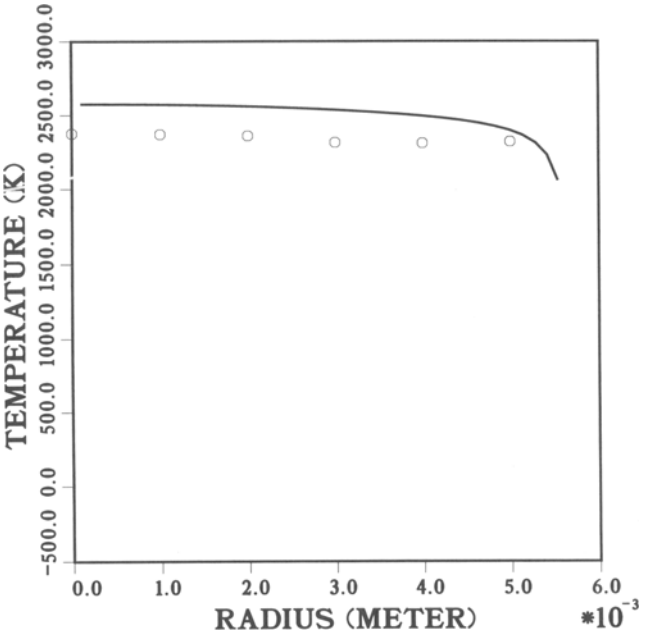


**Fig. 5** Comparison between computational prediction and experimental measurements of the radial distribution of the gas temperature at barrel exit (O, experiment; ——, calculation)

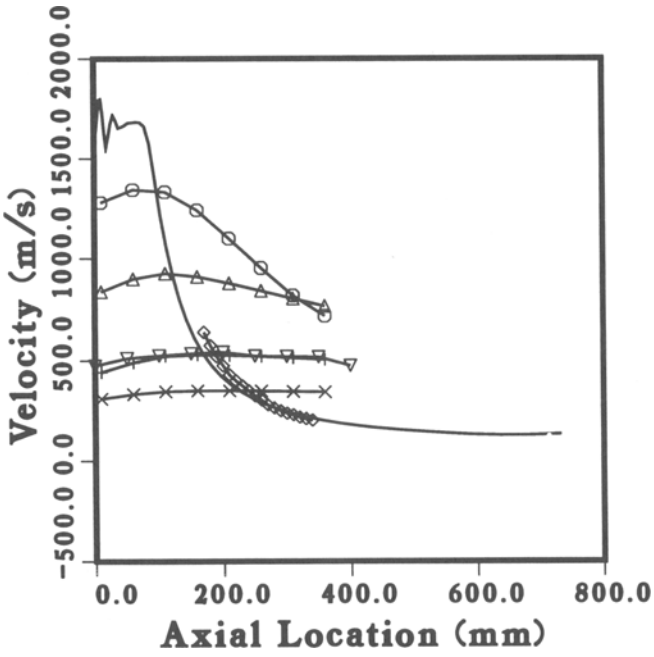


**Fig. 7** Comparison between computational prediction and experimental measurement of gas velocity and particle velocity distribution at the jet centerline for the case of 8 in gun barrel (◊, experiment, gas velocity (Ref 16), ——, calculation, O, 10 μm; Δ, 20 μm; +, 40 μm; ×, 60 μm; ∇, 35 μm experiment particle velocity) (Ref 18)

cause particle size typically ranges from 10 to 60 μm in TS applications, Fig. 7 shows averaged particle velocities for 10, 20, 40, and 60 μm particles as a function of axial location from the exit of the barrel. The simulations were done for Inconel 718 alloy injected at the rate of 10 lb/h into an 8 in. barrel. Gas velocity is shown in the same figure. The 10 μm particles exit the barrel at a high speed of 1250 m/s and continue to accelerate to speeds as high as 1350 m/s at 100 mm from the barrel exit. However, the particles are then decelerated by gas due to a drastic decrease in the gas velocity. Particles end up at about 700 m/s when they reach the substrate at a normal standoff distance of 360 mm from the barrel. The 20 and 40 μm particles exit from the barrel at speeds of about 820 and 470 m/s, respectively. Due to the greater inertia of these particles, they are accelerated less when gas speed is greater than the respective particle speeds. However, these particles also decelerated less when the gas speed decreases to below the corresponding particle speed. Thus, in Fig. 7 at a distance of 360 mm from the exit, the 20 μm particle will have higher velocity than the 10 μm particle. The 60 μm particle exits from the gun at a speed of about 300 m/s and retains that velocity in the jet flow region. At the standoff distance, all four particles have higher velocity than the gas velocity. There is a large variation in particle velocity as a function of particle size. At the typical plating location, the difference is about 400 m/s for 10 and 60 μm particles. This difference translates into an order of magnitude difference in kinetic energy per unit mass of the impinging particle and obviously will lead to different plating conditions. In general, the understanding is that the higher the velocity, the better the coating. It is believed that the greater velocity simply packs the particle more tightly. These velocity differences for different size particles at the same injection speed (20 m/s) can be explained by the particle inertia and hence particle acceleration/deceleration mechanism. The significant influence of particle size on particle dynamics can be quantitatively seen from Eq 5, which shows that particle acceleration and deceleration relaxation time is dependent on the particle diameter-squared.

To compare with experimental results, we also draw average particle velocity along the centerline measured in Ref 19 in Fig. 7.

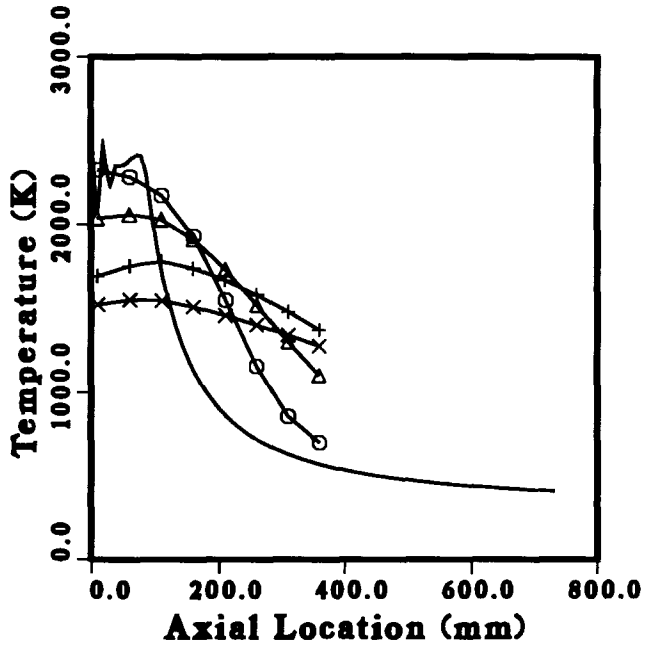


**Fig. 8** Gas and particle temperature distribution at the jet centerline for the case of 8 in. gun barrel (——, gas, O, 10 μm; Δ, 20 μm, +, 40 μm; ×, 60 μm)

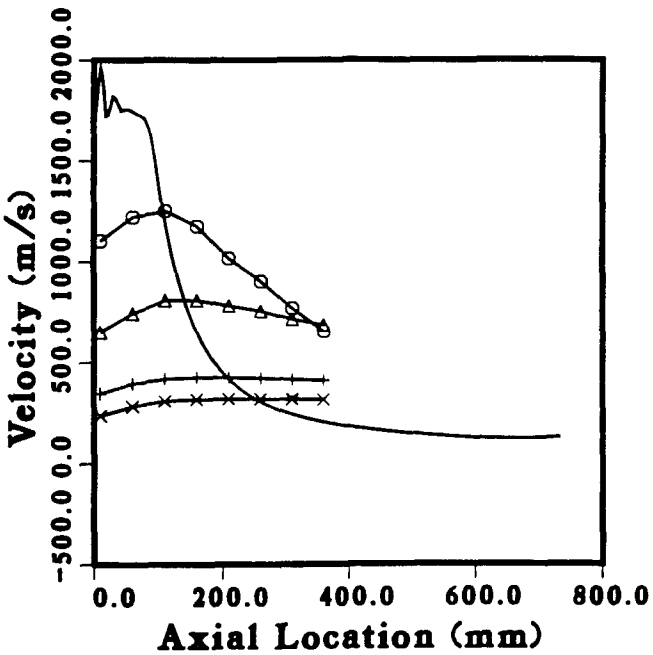


**Fig. 9** Comparison between computational prediction and experimental measurement of gas velocity and particle velocity distribution at the jet centerline for the case of 4 in. gun barrel (——, calculation, O, 10 μm; Δ, 20 μm; +, 40 μm; ×, 60 μm)

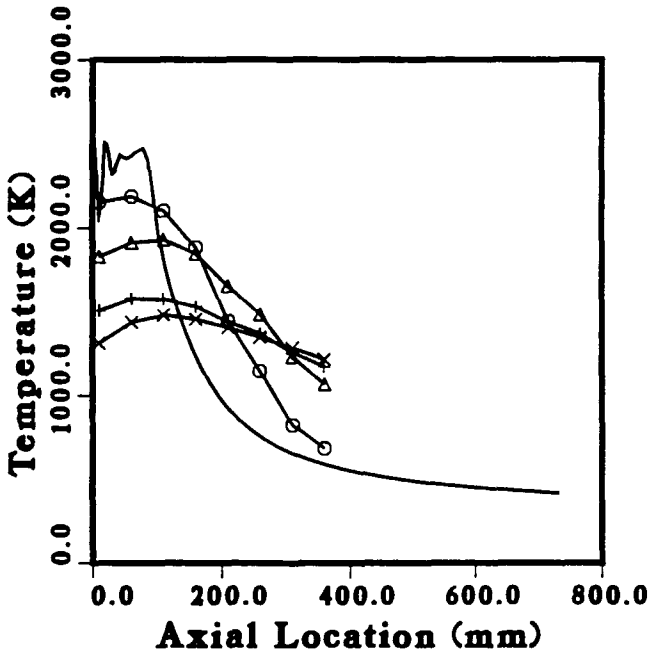


**Fig. 10** Gas and particle temperature distribution at the jet centerline for the case of 4 in gun barrel (——, gas, O, 10 μm; Δ, 20 μm; +, 40 μm; ×, 60 μm)

The number averaged particle size is 35 μm. As we can see, good agreement between experimental measurement and numerical prediction is obtained.

Figure 8 shows particle and gas temperature as a function of axial location. Again, we observe that particle temperatures (except in 10 μm particles, which reach thermal equilibrium at exit of nozzle) rise the first part of the jet, because gas temperature is higher than the particle temperatures. Because the gas temperature decreases sharply in the jet due to gas jet expansion, it drops below particle temperature at the distance of 100 mm from the exit. Particle temperatures are higher than gas temperature at the plating distance. The 10 μm particles almost reach thermal equilibrium with the gas when they reach the exit of the gun. The temperature of 10 μm particles is as high as 2400 K. The 20 μm particles also reach 2000 K at the gun exit. These particle temperatures are well above the melting point of Inconel 718 particles (about 1650 K). Thus, under these conditions, there is a good chance that particles smaller than 20 μm will be deposited

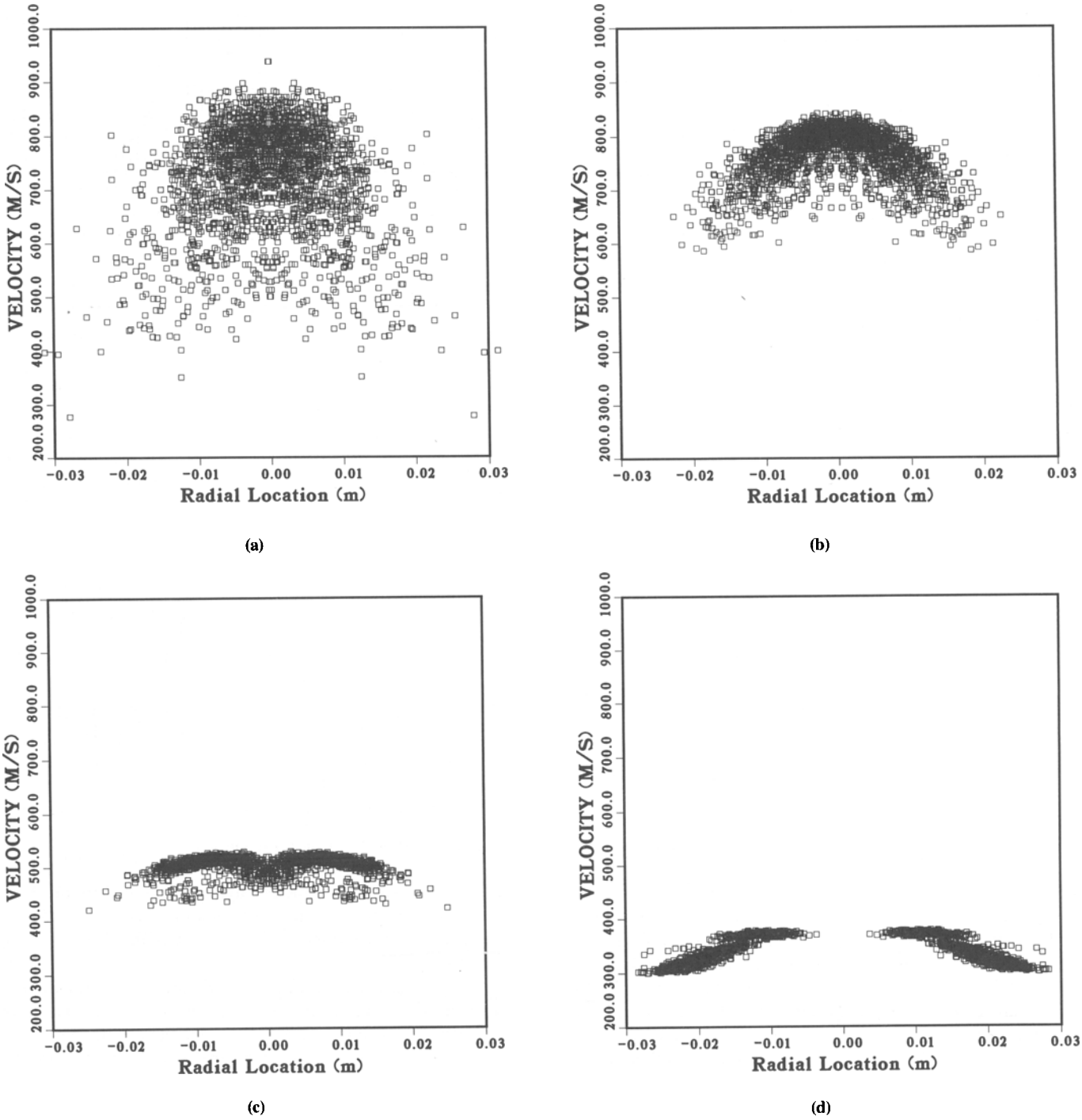


**Fig. 11** Radial particle velocity distribution at standoff distance of 36 mm (a) 10 μm particles (b) 20 μm particles (c) 40 μm particles (d) 60 μm particles

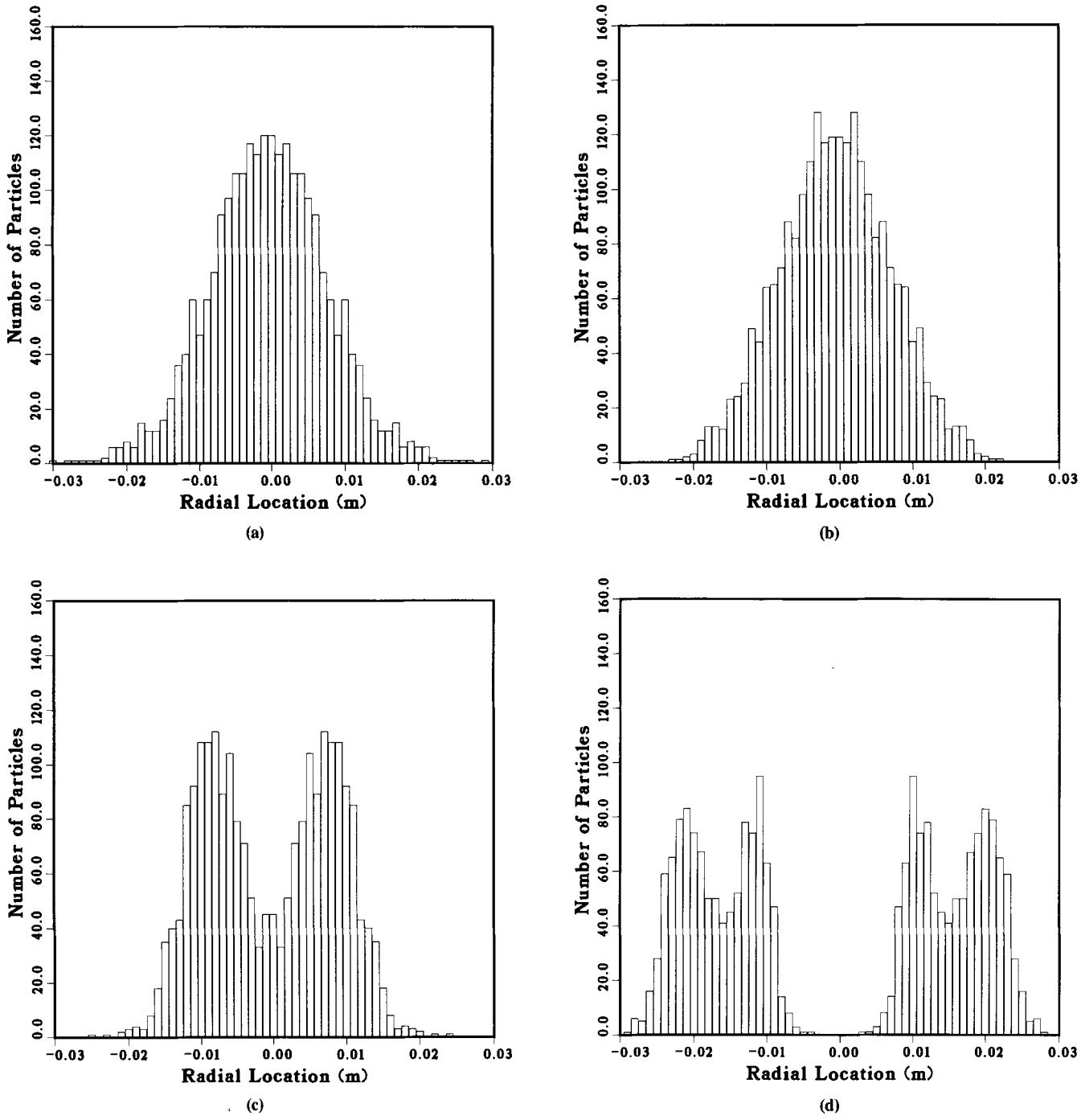


**Fig. 12** Particle concentration distribution at cross section 36 cm from the barrel exit (a) 10 μm. (b) 20 μm. (c) 40 μm (d) 60 μm

at the barrel surface. The temperature of 60 μm particles may be too low to obtain good coating quality, because they may never reach the melting point during the entire process. At the plating distance, the average temperatures for 10, 20, 40, and 60 μm particles are 700, 1100, 1400, and 1300 K, respectively. At the 350 mm plating distance, 40 μm particles have the highest temperature of about 1400 K, whereas the temperature for 10 μm particles dropped to 700 K due to fast cooling of the small particle in the gas. This temperature difference will significantly affect plating quality. This trend again can be demonstrated through Eq 11, which shows that particle heating is proportional to the square of the particle diameter. However, the temperature differences are somewhat smaller between the different-sized particles because of the longer residence time of the slower moving, larger particles.

As we observe from Fig. 7 and 8, larger particles are more difficult to heat and to accelerate. However, they are also more difficult to cool and decelerate. They maintain their velocity and temperature longer and have greater kinetic energy at impact on the substrate. As observed, large differences in velocity and temperature exist for different particle sizes, which lead to the conclusion that optimal coating conditions can be obtained for a

much narrower range of particle sizes than 10 to 60 μm and that a large amount of coating material is wasted.

To study the effect of the gun barrel length on particle velocity and temperature, a second set of simulations was done for a 4 in. barrel gun. The resulting centerline gas velocity averaged particle velocities are shown in Fig. 9. Gas temperature and average particle temperature as a function of axial location from the gun exit is plotted in Fig. 10. In general, we observe the same trend of variation of particle temperature and velocity as the particles travel through the jet. Careful comparison of Fig. 7 and 9 shows that at the gun exits (axial location 0), the particle velocity of each particle size for the 8 in. barrel is higher than the particle velocity of the same size for the 4 in. barrel. This is expected, because the longer the barrel, the longer the time to accelerate the particles. At the plating distance, the particle velocity of each particle size for the 8 in. barrel case is about 50 to 100 m/s higher than the velocity of the same size particle in the 4 in. barrel case. Comparing the particle temperatures of Fig. 8 and 10, we observe the same general trend for particle temperature variations in both the 8 and 4 in. barrel cases. The variations in the particle velocity and temperature as a function of barrel length may well be used to achieve the optimal condition for different coating materials and requirements.

Simulation of particle interaction with flow microturbulence allows us to predict particle parameter distribution in the cross sections of the jet. Figure 11 displays particle velocity distribution as a function of radius at the standoff distance for particle sizes 10, 20, 40, and 60 μm for the case of an 8 in. gun barrel. This figure shows large variations in particle velocity for small particles at the gun exit, because they are more affected by the local turbulence and velocity variation in the cross section. In general, particles exit from the barrel and spread out in a radial direction as they travel downstream. However, we find that the spreading is highly restricted. At a standoff distance of 36 cm, the particle jet spread or the deposition spot is well defined within less than 30 mm diameter. For 10 μm particles, the velocity varies from 70 to 400 m/s; most of the particles have a velocity higher than 600 m/s. For 20 μm particles, the velocity variation is between 600 and 850 m/s. For 40 μm particles, the velocity variation is kept between 400 and 500 m/s. Finally, for 60 μm particles, the velocity variation is in the range of 300 to 375 m/s. In general, "uniform" or "top hat" distribution of particle velocity is desirable for uniform coating. In Fig. 12, the radial cross section of particle density distribution at the standard plating distance (360 mm) is given in the form of particle numbers at the radial locations. The particle distributions are presented for 10, 20, 40, and 60 μm particle sizes. In this figure, we observe that the particle density distribution is a strong function of the particle size. While 10 and 20 μm particles have a typical Gaussian distribution, 40 and 60 μm particles will produce coating spots or "rings" with most of the material concentrating at the edges. Our preliminary simulation results (Ref 19) show changing the particle injection velocity will allow modification of the particle density distribution; however, it will be very difficult to affect all classes of particles at once in the necessary direction. Thus, improving the distribution for the large particles might worsen it for the small particles.

## 4. Conclusion

A two-phase flow numerical model is developed and applied to study an HVOF thermal spraying system. The gas flow field and particle trajectories and temperature histories are calculated and presented. Validation of numerical simulation results with experimental data has shown the CFD methodology accurately predicts gas and particle flow fields in the HVOF TS system. A parametric study is conducted for different particle sizes and gun barrel lengths. The quantitative results obtained by this analysis offer a comprehensive, fundamental analysis of the HVOF thermal spray system. It appears that for the JP-5000 system, particle injection velocity should be carefully controlled in order to produce a high-quality coating. We also have shown that particle trajectories and parameters are very strong functions of the particle radius. The developed methodology allows the researcher or engineer to design optimal injection conditions for different particle and flow regimes. This approach can significantly reduce plating development time for new plating systems and improve the quality of the traditional platings.

### Acknowledgments

The authors would like to thank Dr. A. Tsao and Dr. E. Oran for their encouragement and interest in this project. The authors would also like to express appreciation to Dr. J. Morrison and Dr. T.B. Gatski of NASA Langley Research Center for their contribution to this work. The work reported here was partially supported by ARPA.

### References

1. A.S. Brown, Spraying for Strength, *Aerosp. Am.*, Jan 1992, p 52-56
2. M. Thorpe and H. Richter, A Pragmatic Analysis and Comparison of the HVOF Process, *Thermal Spray Coatings: Research, Design, and Applications*, C.C. Berndt and T.F. Bernecki, Ed., ASM International, 1993, p 157-167
3. E Oberkampf and M. Talpallikar, Analysis of a High Velocity Oxygen-Fuel (HVOF) Thermal Spray Torch, Thermal Spray Industrial Applications, C. Berndt and S Sampath, Ed., ASM International, 1994, p 381-386
4. E. Kadyrov, Y. Evdokimenko, V. Kisel, V Kadyrov, and F. Worzala, Interaction of Particles with Carrier Gas in HVOF Spraying Systems, *J. Therm. Spray Technol.*, Vol 3, 1994, p 389-397
5. C. Crowe and D Stock, A Computer Solution for Two-Dimensional Fluid-Particle Flows, *Int. J. Numer. Methods Eng.*, Vol 19, 1976, p 185-196
6. P.P. Chen and C T. Crowe, On the Monte-Carlo Method for Modeling Particle Dispersion in Turbulence, *Symposium Gas-Solid Flows*, American Society of Mechanical Engineers, 1984, p 37-42
7. H. Speziale, R Abid, and E. Anderson, "A Critical Evaluation of Two-Equation Models for Near Wall Turbulence," Paper 90-1491, American Institute of Aeronautics & Astronautics, 1990
8. J Morrison, "Flux Difference Split Scheme for Turbulent Transport Equations," Paper 90-5251, American Institute of Aeronautics & Astronautics, 1990
9. P.L. Roe, Approximate Riemann Solvers, Parameter Vectors, and Difference Schemes, *J. Compt. Phys.*, Vol 43, 1981, p 357-372
10. D Milojevic, Lagrangian Stochastic-Deterministic (LSD) Prediction of Particle Dispersion in Turbulence, *Part. and Part. System Characterization*, Vol 7, 1990, p 181-190
11. M Sommerfeld, Modeling of Particle/Wall Collision in Confined Gas-Particle Flows, *Int J. Multiphase Flow*, Vol 18, 1992, p 905-926

12 C T Crowe, M P Sharma, and D E Stock, The Particle-Source-In Cell (PSI-CELL) Model for Gas-Droplet Flows, *ASME J. Fluids Eng.*, Vol 99 (No 2), 1977, p 325-332

13 P J Thomas, On the Influence of the Basset History Force on the Motion of a Particle through a Fluid, *Phys. Fluids A*, Vol 4, 1992, p 2090-2093

14 R. Clift, J.R. Grace, and M.E Weber, *Bubbles, Drops and Particles*, Academic Press, 1978

15 I Gary, Higher Velocity Thermal Spray Processes Produce Better Aircraft Engine Coatings, JAE 28th Ann Aerospace/Airline Plating & Metal Finishing Forum & Exposition (San Diego, CA), April 1992

16 W D Swank, J.R Fincke, D C Haggard, and G Irons, HVOF Gas Flow Field Characteristics, *Thermal Spray Industrial Applications*, C Berndt and S. Sampath, Ed., ASM International, 1994, p 313-318

17 S. Gordon and B. McBride, "Computer Program for Calculation of Complex Chemical Equilibrium Compositions, Rocket Performance, Incident and Reflected Shocks, and Chapman-Jouguet Detonations," SP-273, National Aeronautics and Space Administration, May 1976, new version, 1989

18 W.D Swank, J.R Fincke, and D.C Haggard, HVOF Particle Flow Field Characteristics, *Thermal Spray Industrial Applications*, C Berndt and S Sampath, Ed., ASM International, 1994, p 319-324

19 S Eidelman and X. Yang, Optimization of the Thermal Spray Guns and Coating Processes Using Numerical Simulation, Annual Meeting and Exhibition (Anaheim, CA), Feb 1996, TMS